# 72416\_Auto\_Edited - check.docx

7 **Name of Journal:** World Journal of Diabetes

Manuscript NO: 72416

Manuscript Type: ORIGINAL ARTICLE

# Basic Study

Long noncoding RNA X-inactive specific transcript regulates NLR family pyrin domain containing 3/caspase-1-mediated pyroptosis in diabetic nephropathy

LncRNA-XIST regulates RTEC pyroptosis in DN

Jia Xu, Qin Wang, Yifan Song, Xiaohui Xu, He Zhu, Peidan Chen, Yeping Ren

#### Abstract

#### BACKGROUND

NLRP3-mediated pyroptosis is recognized as an essential modulator of renal disease pathology. Long noncoding RNAs (lncRNAs) are active participators of diabetic nephropathy (DN). X inactive specific transcript (XIST) expression has been reported to be elevated in the serum of DN patients.

#### AIM

We aimed to evaluate the mechanism of lncRNA XIST in renal tubular epithelial cell (RTEC) pyroptosis in DN.

#### **METHODS**

A DN rat model was established through streptozotocin injection, and XIST was knocked down by tail vein injection of the lentivirus LV sh-XIST. Renal metabolic and biochemical indices were detected, and pathological changes in the renal tissue were assessed. The expression of indicators related to inflammation and pyroptosis was also detected. High glucose (HG) was used to treat HK2 cells, and cell activity and lactate dehydrogenase (LDH) activity were detected after silencing XIST. The subcellular localization and downstream mechanism of XIST were investigated. Finally, a rescue experiment was carried out to verify that XIST regulates NLR family pyrin domain containing 3 (NLRP3)/caspase-1-mediated RTEC pyroptosis through the microRNA-15-5p (miR-15b-5p)/Toll-like receptor 4 (TLR4) axis.

#### RESULTS

XIST was highly expressed in the DN models. XIST silencing improved renal metabolism and biochemical indices and mitigated renal injury. The expression of inflammation and pyroptosis indicators was significantly increased in DN rats and HG-treated HK2 cells; cell viability was decreased and LDH activity was increased after HG treatment. Silencing XIST inhibited RTEC pyroptosis by inhibiting NLRP3/caspase-1.

Mechanistically, XIST sponged miR-15b-5p to regulate TLR4. Silencing XIST inhibited TLR4 by promoting miR-15b-5p. miR-15b-5p inhibition or TLR4 overexpression averted the inhibitory effect of silencing XIST on HG-induced RTEC pyroptosis.

#### CONCLUSION

Silencing XIST inhibits TLR4 by upregulating miR-15b-5p and ultimately inhibits renal injury in DN by inhibiting NLRP3/caspase-1-mediated RTEC pyroptosis.

**Key Words:** Diabetic nephropathy; Pyroptosis; Renal tubular epithelial cell; Long noncoding RNA X-inactive specific transcript; microRNA-15b-5p; Toll-like receptor 4; NLR family pyrin domain containing 3/caspase-1 pathway

Xu J, Wang Q, Song Y, Xu X, Zhu H, Chen P, Ren Y. Long noncoding RNA X-inactive specific transcript regulates NLR family pyrin domain containing 3/caspase-1-mediated pyroptosis in diabetic nephropathy. *World J Diabetes* 2022; In press

Core Tip: We investigated the mechanism of long noncoding RNA X-inactive specific transcript (XIST) on NLR family pyrin domain containing 3/caspase-1-mediated renal tubular epithelial pyroptosis through the microRNA-15-5p/Toll-like receptor 4 axis and identified XIST as a possible molecular target to mediate renal tubular epithelial pyroptosis in the treatment of renal injury in diabetic nephropathy.

#### INTRODUCTION

As a deleterious complication of diabetes and a critical cause of end-stage renal failure, diabetic nephropathy (DN) mainly manifests as morphological and functional abnormalities, such as glomerular hyperfiltration, natriuresis, proteinuria, the dysregulation of cell junction intercellular communication [1] and changes in the structure and function of the kidneys [2]. DN is characterized by thickening of the glomerular basement membranes, glomerular capillary damage, inflammation and

oxidative stress, mesangium expansion, and urinary microalbumin [3]. The main process crucial for DN pathogenesis is the increased loss of renal cells, which consequentially leads to renal damage and renal dysfunctions involving alterations in structural integrity and glomerular filtration [4]. DN is triggered by many factors, such as dyslipidaemia, hyperglycaemia, haemodynamic abnormalities, and environmental and genetic causes [5,6]. Additionally, evidence accumulated from experimental and clinical studies indicates that renal inflammation is key to determining the progression of renal injury [7]. Despite the high mortality of diabetic patients with DN, effective treatment remains elusive. Identifying genetic determinants and understanding their roles in DN progression is crucial to develop effective diagnostic tools and treatments.

Pyroptosis, a newlydiscovered mode of programmed cell death, is characterized by dependence on caspase-1 and NLRP3 inflammasome activation [8]. The participation of pyroptosis in cancers, cardiovascular diseases, and microbial infection-related diseases has been intensively studied [9-11]. Pyroptosis can cause cell death, inflammation, and renal injury, while inhibiting pyroptosis relieves pathological injury [12, 13]. The involvement and importance of pyroptosis in DN have recently been clarified [14]. Increasing evidence suggests that pyroptosis and the subsequent inflammatory response play key roles in DN pathogenesis [15-17].

Noncoding RNAs (ncRNAs), such as microRNAs (miRNAs), long noncoding RNAs (lncRNAs), and circular RNAs, participate in DN pathogenesis by regulating inflammation, apoptosis, and other pathological processes [18, 19]. A recent study reported that DN progression is closely related to lncRNA expression, which is important for the early diagnosis of DN and targeted interventions [20]. XIST expression is elevated in the serum of DN patients [21]. Silencing XIST protects against renal interstitial fibrosis in DN mice *via* miR-93-5p [22]. XIST also regulates pyroptosis in lung cancer [23], but its effect on renal tubular epithelial cell (RTEC) pyroptosis is unknown. miRNAs are well-known biomarkers used in DN diagnosis, and miRNA profile alterations significantly correlate with DN and renal dysfunction [24]. miR-15b-5p is downregulated in urinary exosomes of DN patients compared with healthy controls [6].

Moreover, the miR-15a-5p-XIST-CUL3 competing endogenous RNA (ceRNA) network is involved in the mechanism of sepsis-induced acute kidney injury [25]. Whether there is a ceRNA loop involving XIST and miR-15b-5p in RTECs in DN progression is largely unknown. Therefore, we studied the mechanism of lncRNA XIST in RTEC pyroptosis and provide a new theoretical basis for XIST as a molecular target to mediate RTEC pyroptosis in DN management.

#### MATERIALS AND METHODS

#### DN model establishment and treatment

Male Sprague-Dawley rats (8 wk, 300~320 g) were provided by Shanghai Experimental Animal Center (Shanghai, China) and raised in a specific pathogen-free animal room at 25°C under a 12/12 h light-dark cycle with free access to food and water. The model was established after one week of adaptive feeding. Streptozotocin (STZ, 50 mg/kg, S0130, Sigma, USA) was used to establish the DN rat model. STZ was dissolved in 0.1 M citric buffer. The DN model was established by (intraperitoneal injection, i.p.) once per day for 5 days. Fasting blood glucose levels were measured 5-7 days after injection, and rats with fasting blood glucose levels above 16.5 mmol/L for 3 consecutive days were identified as successful DN models. Rats in the control group were injected with an equal volume of citrate buffer (P4809, Sigma, USA). The rats were allocated into a control group, DN group, DN + LV-sh-NC group, and DN + LV-sh-XIST group. Each rat was numbered according to its weight and divided into groups according to the random number method. There were 8 rats in each group, for a total of 32 rats. The health status of the rats was monitored every 2 days. If weight loss was > 15%, the rat was euthanized; however, no animals died before the end of the experiment. After successful model establishment (Day 7 after STZ injection), the DN rats were injected with LV-sh-NC or LV-sh-XIST lentiviral interference vectors (200 µL, GenePharma, Shanghai, China). All DN rats were sacrificed by intraperitoneal injection of pentobarbital (100 mg/kg, P-010, Sigma USA) on the 21st day after STZ

injection. All appropriate measures were taken to minimize the pain and discomfort of the animals.

#### Detection of renal metabolic and biochemical indices in rats

The rats were placed in the metabolic cage alone, and urine protein for 24 h (UP 24 h) was collected. On the 20th day after STZ injection, rats in each group were fasted overnight and then weighed. Tail vein blood samples were then analysed by a portable blood glucose meter (OneTouch Ultra Easy, Johnson & Johnson, NJ, USA) to measure fasting blood glucose (FBG). Blood samples were collected from the posterior orbital venous plexus. Serum samples were separated from the blood samples by centrifugation (1000 g, 10 min, 4°Q. The rats were euthanized by excessive pentobarbital (100 mg/kg, i.p.), and the kidney was collected and weighed. KW/BW was calculated according to the following formula: KW/BW = kidney weight (g)/body weight (g).

According to the manufacturer's instructions, blood urea nitrogen (BUN) was detected by a UREA/BUN assay kit (Changchun Huili Biotech, Changchun, China); serum creatinine (Cr) was detected by a Cr assay kit (Huili Biotech); and UP 24 h was detected by an UP assay kit (Nanjing Jiancheng, Nanjing, China). These parameters were analysed with a 240 or 800 Automated Chemistry Analyser (Rayto, Shenzhen, China).

#### Histological staining of kidney tissue

The rats were sacrificed, and the kidneys were collected. The kidneys were fixed with 16 g/L paraformaldehyde solution for 24 h and then embedded in paraffin. Serial sections of 4 µm thickness were cut from paraffined blocks and subjected to haematoxylin and eosin (HE), periodic acid Schiff (PAS), and Masson's trichrome staining and observed under a light microscope (TI-S, Nikon, Japan). The pathological analysis was performed by 2 pathologists unaware of this study using ImageJ (NIH, Bethesda, MD, USA). The glomerular volume was calculated as follows: V = 4/3 m (D/2)<sup>3</sup>, where D is the geometric mean of the four diameters. The mesangial matrix

index was calculated as follows: mesangial matrix index = mesangial matrix area/global area  $\times$  100%. To evaluate tubulointerstitial fibrosis, at least 20 visual fields of each section were analysed by Masson staining software. Scores from 0 to 3 were used to assess the degree of tubulointerstitial fibrosis: 0, normal interstitium; 0.5,  $\leq$  5% of area injured; 1, 5–15% of area injured; 1.5, 16–25% of area injured; 2, 26–35% of area injured; 2.5, 36–45% of area injured; 3, >45% of area injured [26].

### Enzyme-linked immunosorbent assay (ELISA)

Fresh kidney tissue was homogenized in phosphate-buffered saline (PBS) and centrifuged. After total protein quantification, renal tissue samples were used for ELISA measurement  $^{[27]}$ . At the same time, cell culture supernatant was collected. The expression levels of interleukin-1 $\beta$  (IL-1 $\beta$ , RLB00) and IL-18 (DY521-05) in renal tissue and cells were determined according to the ELISA kit instructions (R&D Systems, Minneapolis, MN, USA).

# Western blot analysis

The tissue or cells were lysed with enhanced RIPA lysate (AR0105, Boster, Wuhan, Hubei, China) containing protease inhibitor, and the protein concentration was assessed using a bicinchoninic acid protein quantitative kit (Boster). The protein samples were separated by 10% sodium dodecyl sulfate (SDS)-polyacrylamide gel electrophoresis and transferred to polyvinylidene fluoride membranes. The membranes were then blocked with 5% bovine serum albumin (A1933, Sigma, USA) for 2 h to block nonspecific binding. Next, the membranes were immersed overnight in primary antibody solutions, followed by secondary goat anti-rabbit IgG H&L (HRP) (1:2000, ab205718, Abcam, Cambridge, UK) or goat anti-mouse IgG (1:2000, ab205719, Abcam, Cambridge, UK). The proteins were developed using enhanced chemiluminescence (EMD Millipore, Billerica, MA, USA) and analysed using Image-Pro Plus 6.0 (Media Cybernetics, Silver Spring, MD, USA). The primary antibodies were cleaved caspase-1 (1:1000, #89332, CST, Danvers, MA, USA), caspase-1 (1:100, sc-392736, Santa Cruz Biotechnology, Dallas,

TX, USA), rabbit monoclonal antibody gasdermin D (GSDMD, 1:1000, ab219800, Abcam, Cambridge, UK), GSDMD-N (1:1000, PA5-116815, Thermo Fisher, Waltham, MA, USA), NLRP3 (1:1000, ab214185, Abcam, Cambridge, UK), ASC mouse monoclonal antibody (1:100, sc-514414, Santa Cruz Biotechnology, TX, USA), TLR4 rabbit polyclonal antibody (1:500, ab13867, Abcam, Cambridge, UK), and GAPDH (1:2500, ab9485, Abcam, Cambridge, UK).

#### Immunofluorescence

The kidney was placed on a clean workbench, and the fibrous capsule was stripped using an aseptic technique. Next, 1 cm³ of renal tubular epithelial tissue was removed from the outer skin tissue, washed with normal saline, and fixed with 10% formalin. Sections 4 µm thick were incubated overnight with caspase-1 mouse monoclonal antibody (1:50, sc-392736, Santa Cruz Biotechnology) at 4°C, and then conjugated with secondary goat anti-mouse IgG (Alexa Fluor® 488) (1:200, ab150113, Abcam, Cambridge, UK) in the dark for 1 h. After washing in PBS, the slides were incubated with 4′,6-diamidino-2-phenylindole (DAPI) (D9542, Sigma, USA) for 3 min, followed by glycerine loading. The fluorescence was evaluated under a fluorescence microscope (Olympus Life Sciences, Tokyo, Japan).

# Cell culture and transfection

The human tubular endothelial cell line HK2 from ATCC (Rockville, MD, USA) was cultured in RPMI 1640 medium (Life Technologies, Carlsbad, CA, USA) containing 10% (v/v) foetal bovine serum (FBS, F2442; Sigma, St. Louis, Missouri, USA) at 37°Gwith 50 mL/L CO<sub>2</sub>. After 24 h of starvation in serum-free medium, HK2 cells were cultured in normal (5 mmol/L, NG) or high (40 mmol/L, HG) glucose (Y0001745, Sigma, USA) for 48 h [28].

The miR-15b-5p mimic and miR-15b-5p inhibitor, siRNA sequence targeting XIST (si-XIST), overexpression TLR4 plasmid (oe-TLR4), and their corresponding controls

were provided by GenePharma (Shanghai, China). The cells were transfected using Lipofectamine 2000 (Invitrogen, Carlsbad, CA, USA).

si-XIST sequences were follows: si-XIST-1 (SS sequence: GGAAGUACCUACUACUUAAGA, AS Sequence: si-XIST-2 (SS UUAAGUAGUAGGUACUUCCAG), sequence: GGUGGACUAUCAACAUAUAAU, AS sequence: UAUAUGUUGAUAGUCCACCAG), and si-XIST-3 (SS sequence: AS GGAAAUAGAUAAAUGUCAAAG, sequence: UUGACAUUUAUCUAUUUCCUU).

### Quantitative real-time polymerase chain reaction (qRT-PCR)

Total RNA was extracted using the RNeasy Mini Kit (Qiagen, Valencia, CA, USA). A reverse transcription kit (RR047A, Takara, Tokyo, Japan) was used to obtain cDNA. A miRNA first-strand cDNA synthesis kit (B532451-0020, Sangon, Shanghai, China) was used for miRNA detection.

SYBR Premix Ex Taq II (DRR081, Takara) and real-time fluorescence qPCR (7500, ABI, Foster City, CA, USA) were used for the qRT-PCR experiment. The PCR primers (Table 1) were designed and synthesized by Sangon. GAPDH or U6 was the internal reference. Gene expression was calculated using the  $2^{-\Delta\Delta t}$  method.

#### Cell activity measurement

The viability of HK2 cells was detected by a Cell Titer Glo Luminescent Cell Viability Assay Kit (G7570, Promega, Beijing, China). Cells (10<sup>5</sup>) were seeded into 6-well plates containing normal growth medium and then collected when the confluence reached 80-90%. Before collecting the HK2 cells, the reagents were prepared, and then the cells (50 μL) were loaded into black-walled 96-well plates that contained the same amount of final substrate solution. After mixing for 10 min, the cells were incubated in a plate-reading luminometer (Varioskan<sup>TM</sup>, Thermo Scientific, Rockford, IL, USA).

# Lactate dehydrogenase (LDH) release assay

An LDH release assay kit (Beijing, Nanjing, China) was used to detect cytotoxicity. HG-treated HK2 cells were plated into 96-well plates and incubated at 37°Gwith 50 mL/L CO<sub>2</sub> for 24 h. The cell medium was then collected, and LDH activity was measured.

# Fluorescence in situ hybridization (FISH)

FISH was used to identify the subcellular localization of XIST in HK2 cells. In accordance with the instructions of the Ribo<sup>TM</sup> lncRNA FISH probe mix (Red) (RiboBio, Guangzhou, Guangdong, China), the cover glass was placed into the 6-well culture plate, and HK2 cells were seeded onto it. The confluence was approximately 80% after 1 day of culture. The slides were then washed with PBS and fixed with 1 mL of 16 g/L paraformaldehyde. The slides were treated with proteinase K (2 μg/mL), glycine, and ethylphthalein reagent and then incubated with 250 μL of prehybridizing solution at 42°Cfor 1 h. Next, the prehybridizing solution was removed, and 250 μL of hybridizing solution containing probe (300 ng/mL) was added to the slides for hybridization at 42°C overnight. Following 3 washes with PBS containing 0.05% (v/v) Tween-20 (PBST), DAPI (1:800) diluted with PBST was added to stain the nuclei; the slides were then transferred to 24-well culture plates and incubated for 5 min. The slides were then sealed using an anti-fluorescence quenching agent and photographed using a fluorescence microscope (Olympus) [29].

# Nuclear/Cytosol fractionation

HK2 cells were resuspended in hypotonic buffer A [10 mm HEPES (pH 7.5), 0.5 mm DTT, 10 mmol/L KCl, 1.5 mmol/L MgCl<sub>2</sub>] containing protease inhibitor and RNase inhibitor (N8080119, Thermo Fisher Scientific). The HK2 cells were then incubated on ice for 10 min and centrifuged ( $1000 \times g$ ,  $4^{\circ}$ C, 10 min). The supernatant was further centrifuged at  $15000 \times g$  for 15 min to obtain the cytoplasmic component. The precipitate was washed twice with hypertonic buffer, resuspended in hypotonic buffer B [10 mm HEPES (pH 7.5), 10 mmol/L KCl, 1.5 mmol/L MgCl2, 0.5 mm DTT, 0.5%

Nonidet P-40], incubated at 4°C for 30 min, and then centrifuged at  $6000 \times g$ , 4°C and for 10 min. The precipitate was rinsed once with hypertonic buffer and resuspended in RIPA buffer containing protease inhibitor and RNase inhibitor [50 mm Tris HCl (pH 7.5), 1500 mmol/L KCl, 1% Nonidet P-40, 0.5% sodium hydroxide, 0.1% SDS, 1 mmol/L EDTA, pH 8.0], incubated at 4°C for 30 min, rotated gently, and then centrifuged at 15000 × g for 20 min. The supernatant contained the nuclei [30].

#### Dual-luciferase assay

The binding sites of XIST and miR-15b-5p, miR-15b-5p and TLR4 were predicted by the bioinformatics website StarBase (<a href="http://starbase.sysu.edu.cn/index.php">http://starbase.sysu.edu.cn/index.php</a>). The binding site sequences or their mutants were amplified and inserted into the pmiR vector (Huayueyang, Beijing, China) to construct the wild-type (WT) or mutant (MUT) vectors XIST-WT, TLR4-WT, XIST-MUT, and TLR4-MUT. Subsequently, HEK293T cells (Beinuo, Shanghai, China) were cotransfected with mimic NC or miR-15b-5p mimic for 48 h, after which the cells were collected and lysed, and the luciferase activity was detected using a kit (K801-200; Biovision, Mountain View, CA, USA).

#### RNA immunoprecipitation (RIP)

The binding of miR-15b-5p to TLR43 and XIST was detected by an RIP kit (Millipore, MA, USA). HK2 cells were rinsed with precooled PBS, and the supernatant was discarded. The cells were incubated with an equal volume of RIPA lysate (P0013B, Beyotime, Shanghai, China) for 5 min and centrifuged at 4°C for 10 min to obtain the supernatant. One part of the cell extract was taken as input, and the other part was incubated with the antibody for coprecipitation. RNA was extracted from the sample after detachment with proteinase K and used for qRT-PCR of XIST, miR-15b-5p, and TLR4. The antibodies used in RIP were AGO2 (1:100, ab32381, Abcam, Cambridge, UK) and rabbit anti-IgG (1:100, ab109489, Abcam, Cambridge, UK), which was used as the control.

# Statistical analysis

The statistical review of the study was performed by a biomedical statistician. SPSS 21.0 (IBM Corp. Armonk, NY, USA) was used to process the data, and GraphPad Prism 8.0 (GraphPad Software, San Diego, CA, USA) was used for mapping. All measurement data were tested for normal distribution and homogeneity of variance and are presented as the mean  $\pm$  standard deviation (SD). The comparisons among multiple groups were conducted by one-way or two-way analysis of variance (ANOVA), followed by Tukey's multiple comparisons test. A probability value of p < 0.05 implied a statistically significant difference.

# **RESULTS**

### Silencing lncRNA XIST inhibits STZ-induced renal injury in DN rats

An increasing number of studies have focused on the regulatory mechanism of lncRNAs in DN development. XIST is upregulated in acute kidney injury, and inhibiting XIST can alleviate acute kidney injury [31]. However, the regulatory mechanism of XIST in DN requires further exploration.

To study the role of XIST in DN, we first established a DN rat model and detected XIST expression. XIST in the DN group was higher than that in the control group. We then used LV-sh-XIST lentivirus to knock down XIST expression in the model rats (p < 0.05, Fig. 1A) and detected the renal metabolic and biochemical indices (including KW/BW, FBG, BUN, Cr, and UP 24 h) of the rats. The KW/BW, FBG, BUN, Cr, and UP 24 h values in the DN rats were higher than those in control rats, while LV-sh-XIST injected via the caudal vein significantly reduced these indices (except for FBG) (all p < 0.05, Fig. 1B-F). Meanwhile, we detected the histological changes in renal tissue by HE staining, PAS staining, and Masson staining. Compared with the control group, the DN and DN + LV-sh-NC groups had several abnormalities, such as glomerular hypertrophy, basement membrane thickening, mesangial hyperplasia, glomerular epithelial cell swelling, lumen stenosis, inflammatory cell infiltration, and moderate

fibrosis. Lentivirus LV-sh-XIST intervention improved all of these histological changes (p < 0.05, Fig. 1G). Thus, silencing XIST can inhibit renal injury in DN rats.

# Silencing XIST inhibits pyroptosis in DN rats

Inflammation is an important pathogenic factor of DN that can lead to RTEC pyroptosis <sup>[28]</sup>. However, no studies have investigated the effects of XIST on pyroptosis in DN. Here, we detected IL-1 $\beta$  and IL-18 expression in renal tissue. ELISA revealed that IL-1 $\beta$  and IL-18 in the DN group were elevated, but they were lowered after silencing XIST (p < 0.05, Fig. 2A). Western blot analysis showed that the NLRP3, ASC, cleaved caspase-1, caspase-1, GSDMD, and GSDMD-N levels in the DN group were significantly enhanced, but they were lowered after silencing XIST (all p < 0.05, Fig. 2B). The caspase-1 immunofluorescence results were consistent with the Western blot results (p < 0.05, Fig. 2C). These results suggest that silencing XIST in DN can prevent RTEC pyroptosis.

# Silencing XIST inhibits pyroptosis in HG-induced HK2 cells

HK2 cells were treated with HG to further study the regulatory effect of XIST on RTEC pyroptosis *in vitro*. qRT-PCR found that HG treatment induced high XIST expression, while XIST was significantly decreased after transfection of a siRNA sequence targeting XIST (p < 0.05, Fig. 3A). Si-XIST-1, which had the best silencing efficiency, was used in subsequent experiments. Next, we examined the effect of silencing XIST on RTEC pyroptosis after HG treatment. HG treatment significantly promoted the expression of IL-1 $\beta$  and IL-18 (as detected by ELISA), as well as NLRP3, ASC, cleaved caspase-1, caspase-1, GSDMD, and GSDMD-N (as shown by Western blot), while these levels were significantly lower after silencing XIST (all p < 0.05, Fig. 3B-C). Silencing XIST also annulled the inhibition of HK2 cell viability by HG (p < 0.05, Fig. 3D) and significantly reduced the release rate of LDH (p < 0.05, Fig. 3E). Overall, silencing XIST inhibited HG-induced RTEC pyroptosis *in vitro*.

#### LncRNA XIST binds to miR-15b-5p in DN

To further study the regulatory mechanism of XIST on RTEC pyroptosis in DN, we first used FISH and nuclear/cytosolic fractionation to identify that XIST was mainly expressed in the cytoplasm (Fig. 4A-B). These results indicated that XIST may play a role in DN via a ceRNA loop. StarBase (http://starbase.sysu.edu.cn/index.php) predicted that XIST can bind to miR-15b-5p (Fig. 4C). The dual-luciferase experiment (p < 0.05, Fig. 4D) and RIP experiment verified that XIST could adsorb and bind to miR-15b-5p (p < 0.05, Fig. 4E). qRT-PCR showed that miR-15b-5p in the DN group was significantly lower and was increased after silencing XIST (p < 0.05, Fig. 4F). Moreover, miR-15b-5p in HK2 cells was inhibited by HG treatment and was significantly enhanced after silencing XIST (p < 0.05, Fig. 4G). There was no significant difference in the expression of premiR-15b in rats and cells in each group. These results show that XIST can adsorb and bind to miR-15b-5p to reduce miR-15b-5p expression in DN.

# Inhibition of miR-15b-5p in XIST-silenced HK2 cells activates RTEC pyroptosis

Next, we carried out functional rescue experiments to verify the above regulatory mechanism. We silenced both XIST and miR-15b-5p in HG-exposed HK2 cells. First, we detected miR-15b-5p expression by qRT-PCR, which verified the transfection efficiency of the miR-15b-5p inhibitor (p < 0.05, Fig. 5A). In HG-treated HK2 cells, the miR-15b-5p inhibitor reversed the inhibitory effect of si-XIST on IL-1 $\beta$  and IL-18 (all p < 0.05, Fig. 5B); it also reversed the expression of NLRP3, ASC, cleaved caspase-1, caspase-1, GSDMD, and GSDMD-N (all p < 0.05, Fig. 5C). Compared with the si-XIST + inhibitor NC group, the cell activity of the si-XIST + miR-15b-5p inhibitor group was decreased (p < 0.05, Fig. 5D), while the release rate of LDH was increased (p < 0.05, Fig. 5E). Taken together, these results indicate that silencing XIST inhibits HG-induced RTEC pyroptosis *in vitro* by promoting miR-15b-5p.

#### LncRNA XIST sponges miR-15b-5p to inhibit TLR4

To study the downstream mechanism of miR-15b-5p, we utilized the StarBase website (http://starbase.sysu.edu.cn/index.php) to predict that miR-15b-5p can bind to the

3'UTR of TLR4 (Fig. 6A). The dual-luciferase assay and RIP assay also showed that TLR4 was the direct target gene of miR-15b-5p (p < 0.05, Fig. 6B-C). TLR4 expression in renal tissue was assessed by qRT-PCR and Western blot. The results showed that TLR4 in renal tissue of the DN group was higher than that of the control group, and TLR4 was lower after silencing XIST (all p < 0.05, Fig. 6D-E). Additionally, silencing XIST significantly reversed the TLR4 expression induced by HG, while the miR-15b-5p inhibitor reversed the inhibitory effect of silencing XIST (all p < 0.05, Fig. 6F-G). In summary, XIST inhibits TLR4 expression by binding to miR-15b-5p.

## TLR4 overexpression in XIST-silenced cells causes increased pyroptosis

TLR4 promotes apoptosis by activating NLRP3/caspase-1 in hepatic ischaemia-reperfusion injury [32]. Whether XIST regulates HG-induced RTEC pyroptosis through TLR4 remains to be explored.

To further verify the regulatory effect of XIST on TLR4, we silenced XIST and overexpressed TLR4 in HG-treated HK2 cells and detected the TLR4 Levels. TLR4 was significantly overexpressed (p < 0.05, Fig. 7A-B). Compared with the si-XIST + oe-NC group, TLR4 overexpression promoted IL-1 $\beta$  and IL-18 expression and increased the levels of NLRP3, ASC, cleaved caspase-1, caspase-1, GSDMD, and GSDMD-N (all p < 0.05, Fig. 7C-D). Furthermore, TLR4 overexpression decreased cell viability (p < 0.05, Fig. 7E) and increased the release rate of LDH (p < 0.05, Fig. 7F). In summary, silencing XIST inhibits HG-induced RTEC pyroptosis by inhibiting TLR4.

#### **DISCUSSION**

As the most prevalent, disastrous, and costly complication of diabetes, DN occurs in approximately 30% to 40% of diabetic patients, representing a considerable public health problem [33]. Pyroptosis and the subsequent inflammatory response are dominant events in DN pathogenesis [15]. This study found that DN induces RTEC pyroptosis by activating NLRP3/caspase-1 and inducing high XIST expression. Silencing XIST promoted the targeted inhibition of TLR4 by miR-15b-5p by upregulating miR-15b-5p,

thus inhibiting TLR4 and finally alleviating renal injury in DN rats by inhibiting NLRP3/caspase-1-mediated RTEC pyroptosis (Fig. 8).

XIST silencing has been shown to alleviate certain biological processes and inflammation in HG-treated human mesangial cells (HMCs) [21]. XIST was found to be highly expressed in renal tissue of DN patients, STZ-treated DN mice, and HG-exposed HK-2 cells [22]. Consistently, the STZ (50 mg/kg)-induced DN rat model in our study showed the upregulation of XIST. XIST expression was downregulated by LV-sh-XIST lentivirus, and renal metabolic and biochemical indices were detected. The results showed that LV-sh-XIST significantly reduced the values of KW/BW, BUN, Cr, and UP 24 h. FBG is a highly related indicator of diabetes. XIST silencing can improve the symptoms of diabetic nephropathy but cannot completely cure diabetes. Correspondingly, our results showed that FBG was not restored after XIST silencing. One study showed that a markedly elevated FBG content in the serum of DN rats indicated seriously disordered glucose metabolism; the DN rats also presented elevated BUN and Cr levels, which were associated with impaired renal filtration function [34]. As previously noted, the metabolic burden caused by hyperglycaemia can result in metabolic injuries, such as tissue inflammation, glomerular filtration, tubular hypertrophy, and tissue fibrosis [35]. In the current study, histological staining of renal tissue demonstrated that the DN rats showed glomerular hypertrophy, basement membrane thickening, mesangial hyperplasia, glomerular epithelial cell swelling, lumen stenosis, inflammatory cell infiltration, and fibrosis; however, LV-sh-XIST intervention improved these histological changes. Preventing glomerular hypertrophy and attenuating glomerular hyperfiltration may have therapeutic potential for DN [35]. Consistently, prior work suggests that XIST knockdown alleviates acute kidney injury [31]. These results suggest that silencing IncRNA XIST can inhibit renal injury in DN rats.

Inflammation and RTEC pyroptosis are hallmarks of tubular cell damage and renal functional deterioration in kidney injury [36]. The urinary level of the inflammatory mediator IL-18 has been reported to be positively linked with DN progression [37]. The participation of pyroptosis in DN progression has recently attracted much attention [38,

<sup>28]</sup>, and we investigated inflammation and RTEC pyroptosis-related factors. Our results revealed that the IL-1β and IL-18 levels in DN rats were elevated, but they were lower after silencing XIST. Western blot and caspase-1 immunofluorescence showed that the NLRP3, ASC, caspase-1, and GSDMD levels in the DN group were enhanced, but they were lower after silencing XIST, which was highly consistent with previous studies [39, 34]. NLRP3 inflammasome activation is related to cell pyroptosis [40]; therefore, the inhibition of NLRP3 inflammatory bodies may be a potential option for DN treatment [41]. To further study the regulatory effect of XIST on pyroptosis, HK2 cells were treated with HG to further study the regulatory effect of XIST on RTEC pyroptosis *in vitro*. Our results revealed that silencing XIST inhibited HG-induced RTEC pyroptosis *in vitro*, reversed the inhibitory effect of HG on HK2 cell viability, and reduced the release rate of LDH. Podocytes exposed to 30 mM HG showed significantly elevated levels of caspase-11, GSDMD-N, IL-1β, and IL-18, indicating that pyroptosis is activated under hyperglycaemic conditions and during DN development [14]. Collectively, the results indicate that silencing XIST in DN can inhibit HG-induced RTEC pyroptosis.

To further study the regulatory mechanism of XIST on RTEC pyroptosis in DN, we used FISH and nuclear/cytosolic fractionation to identify that XIST was mainly expressed in the cytoplasm. These results suggest that XIST plays a role in DN by regulating ceRNAs. StarBase predicted that XIST can bind to miR-15b-5p, which was validated by dual-luciferase experiments and RIP. qRT-PCR showed that miR-15b-5p in the DN models was significantly lower but increased after silencing XIST. Accordingly, miR-15b-5p was found to be downregulated in the serum of DN patients and in HG-treated HMCs [42]. XIST can adsorb and bind to miR-15b-5p to reduce miR-15b-5p expression in DN. We did not investigate whether XIST undergoes nuclear translocation in the DN models or in HG-treated HK-2 cells. We will focus on this question in future research to provide a more comprehensive mechanism for the role of XIST in DN.

We next carried out functional rescue experiments to verify the postulated regulatory mechanism. XIST and miR-15b-5p were both silenced in HG-treated HK2

cells. Accordingly, the miR-15b-5p inhibitor significantly reversed the inhibitory effect of si-XIST on IL-1β, IL-18, NLRP3, ASC, caspase-1, and GSDMD; the cell activity was decreased, while the release rate of LDH was significantly increased. Similarly, a previous study revealed that forced expression of miR-15b-5p restrained HG-triggered apoptosis of podocytes and inflammatory responses and repressed oxidative stress damage [43]. The miR-15b-5p mimic repressed the viability and inflammation of HG-treated HMCs, as previously shown [42]. The findings show that silencing XIST inhibits HG-induced RTEC pyroptosis *in vitro* by promoting miR-15b-5p. As yet, there have been no studies on the correlation between miR-15b-5p and RTEC pyroptosis in DN, indicating the novelty of our findings.

To study the downstream mechanism of miR-15b-5p, the StarBase website was used to predict that miR-15b-5p can bind to TLR4, which was validated by a dualluciferase assay and RIP assay. qRT-PCR and Western blotting showed that TLR4 in the DN models was significantly enhanced but was lower after silencing XIST. The miR-15b-5p inhibitor mitigated the inhibition of TLR4 when XIST was silenced. In summary, XIST inhibits TLR4 by binding to miR-15b-5p. RTEC pyroptosis-induced tubular injury is accompanied by upregulated TLR4 and GSDMD in DN patients [44]. To further verify that the regulation of RTEC pyroptosis by XIST is realized through TLR4, we silenced XIST and overexpressed TLR4 in HG-treated HK2 cells. As expected, TLR4 overexpression promoted IL-1β, IL-18, NLRP3, ASC, cleaved caspase-1, caspase-1, GSDMD, and GSDMD-N; decreased cell activity; and increased the release rate of LDH. The results of several studies support our findings. TLR4 promotes apoptosis by activating NLRP3/caspase-1 [32]. TLR4 depletion inhibits microglial pyroptosis to promote motor function recovery after spinal cord injury [45]. The TLR4 inhibitor TAK-242 induced GSDMD-mediated pyroptosis in HG-exposed cells [44]. In summary, silencing XIST inhibits HG-induced RTEC pyroptosis by inhibiting TLR4.

#### **CONCLUSION**

Overall, our results indicate that silencing XIST ultimately relieves renal injury in DN by inhibiting NLRP3/caspase-1-mediated RTEC pyroptosis *via* the ceRNA network of eXIST/miR-15b-5p/TLR4. However, the mechanism of abnormal XIST and miR-15b-5p expression in renal injury in DN has not been comprehensively studied and will be further explored in our future studies. There are many pyroptosis regulatory mechanisms, among which the classical caspase-1 inflammatory body pathway is the most studied. This pathway includes NLRP1, NLRP3, and other nod-like receptor family inflammatory bodies. Here, we investigated the classical caspase-1 pathway. Many studies have shown that the caspase-11 pathway plays an important role in inflammation-related diseases [14, 46, 47]. We will further explore whether XIST has a regulatory effect on the caspase-11 pathway in future research.

# 72416\_Auto\_Edited - check.docx

ORIGINALITY REPORT

5%

SIMILARITY INDEX

#### **PRIMARY SOURCES**

- Ruiqiong Ke, Yan Wang, Shihua Hong, Lixia Xiao. "Endoplasmic reticulum stress related factor IRE1 $\alpha$  regulates TXNIP/NLRP3-mediated pyroptosis in diabetic nephropathy", Experimental Cell Research, 2020 Crossref
- 2 pubs.rsc.org 32 words 1 %
- www.ncbi.nlm.nih.gov 28 words < 1 %
- Jindou Yang, Yan Shen, Xia Yang, Yanjun Long, Shuang Chen, Xin Lin, Rong Dong, Jing Yuan.

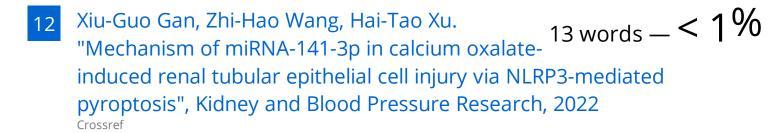
  "Silencing of long noncoding RNA XIST protects against renal interstitial fibrosis in diabetic nephropathy via microRNA-93-5p-mediated inhibition of CDKN1A", American Journal of Physiology-Renal Physiology, 2019

  Crossref
- Jian Sun, Yang Wang, Lei Niu, Lujia Tang, Shuming 18 words <1% Pan. "USF2 Knockdown Downregulates THBS1 to Inhibit the TGF-β Signaling Pathway and Reduce Pyroptosis in Sepsis-Induced Acute Kidney Injury", Research Square, 2020 Crossref Posted Content
- Jianzhao Liao, Zhuoying Hu, Quanwei Li, Hongji Li et al. " Endoplasmic Reticulum Stress Contributes 18 words < 1%

to Copper-Induced Pyroptosis Regulating the IRE1α-XBP1 Pathway in Pig Jejunal Epithelial Cells ", Journal of Agricultural and Food Chemistry, 2022

Crossref

- f6publishing.blob.core.windows.net  $\frac{17 \text{ words}}{1}$
- Guanhua Xu, Lujiao Mo, Channi Wu, Xiaoyuan Shen, Hongliang Dong, Lingfeng Yu, Ping Pan, Kanda Pan. "The regulatory axis is important for sepsisinduced acute kidney injury ", Renal Failure, 2019
- Aziz Eftekhari, Sepideh Zununi Vahed, Taras Kavetskyy, Maryam Rameshrad et al. "Cell junction proteins: Crossing the glomerular filtration barrier in diabetic nephropathy", International Journal of Biological Macromolecules, 2020 Crossref
- Dong-Wei Liu, Jia-Hui Zhang, Feng-Xun Liu, Xu-Tong Wang, Shao-Kang Pan, Deng-Ke Jiang, Zi-Hao Zhao, Zhang-Suo Liu. "Silencing of long noncoding RNA PVT1 inhibits podocyte damage and apoptosis in diabetic nephropathy by upregulating FOXA1", Experimental & Molecular Medicine, 2019
- Hong Xing Zheng, Shan Shan Qi, Jia He, Ching Yuan Hu, Hao Han, Hai Jiang, Xin Shen Li. "Cyanidin-3-glucoside from Black Rice Ameliorates Diabetic Nephropathy via Reducing Blood Glucose, Suppressing Oxidative Stress and Inflammation, and Regulating Transforming Growth Factor  $\beta$ 1/Smad Expression", Journal of Agricultural and Food Chemistry, 2020 Crossref



13 www.nature.com

- 13 words -<1%
- Hong Ding, Mohamad Aljofan, Chris R. Triggle. "Oxidative stress and increased eNOS and NADPH oxidase expression in mouse microvessel endothelial cells", Journal of Cellular Physiology, 2007 Crossref
- molecular-cancer.biomedcentral.com

$$_{12 \text{ words}} - < 1\%$$

EXCLUDE QUOTES ON EXCLUDE BIBLIOGRAPHY ON

**EXCLUDE MATCHES** 

< 12 WORDS